PPPL-2181

UC20-F

CHARGE EXCHANGE RECOMBINATION SPECTROSCOPY AS A PLASMA DIAGNOSTIC TOOL

BY

R. J. Fonck

DECEMBER 1984

PLASMA PHYSICS LABORATORY

PRINCETON UNIVERSITY
PRINCETON, NEW JERSEY

PREPARED FOR THE U.S. DEPARTMENT OF ENERGY,
UNDER CONTRACT DE-AC02-76-CHO-3073.

NOTICE

Printed in the United States of America

Available from:

National Technical Information Service
U.S. Department of Commerce
5285 Port Royal Road
Springfield, Virginia 22161

Price Printed Copy $ * ; Microfiche $4.50

*Pages	NTIS Selling Price
1-25	$7.00
25-50	$8.50
51-75	$10.00
76-100	$11.50
101-125	$13.00
126-150	$14.50
151-175	$16.00
176-200	$17.50
201-225	$19.00
226-250	$20.50
251-275	$22.00
276-300	$23.50
301-325	$25.00
326-350	$26.50
351-375	$28.00
376-400	$29.50
401-425	$31.00
426-450	$32.50
451-475	$34.00
476-500	$35.50
500-525	$37.00
526-550	$38.50
551-575	$40.00
567-600	$41.50

For documents over 600 pages, add $1.50 for each additional 25-page increment.

CHARGE EXCHANGE RECOMBINATION SPECTROSCOPY AS A PLASMA DIAGNOSTIC TOOL

Raymond J. Fonck

Plasma Physics Laboratory, Princeton University
Princeton, N.J. 08544

PPPL--2181

DE85 005342

ABSTRACT

Intensity and line profile measurements of the spectra of light hydrogenic ions which are excited by charge exchange reactions with fast neutral atoms are being widely used as diagnostics for fusion plasma research. This technique, which is referred to as charge exchange recombination spectroscopy, allows measurements of the densities of fully stripped impurity ions and particle transport coefficients with only minor uncertainties arising from atomic processes. The excitation of long wavelength transitions in light ions such as He^{+}, C^{5+}, and O^{7+} allows relatively easy measurements of ion velocity distributions to determine ion temperatures and plasma rotation velocities. Among its advantages for such measurements are the facts that fiber optic coupling between a remote spectrometer and the immediate reactor environment is possible in many cases. The measurement is localized by the intersection region of a neutral beamline and viewing sightline, and intrinsic ions can be used so that injection of potentially perturbing impurities can be avoided. A particularly challenging application of this technique lies in the diagnosis of alpha particles expected to be produced in the present generation of $Q \approx 1$ tokamak experiments.

I. INTRODUCTION

The use of charge exchange recombination spectroscopy (CXRS) as a means of actively probing the properties of magnetically confined high temperature plasmas has expanded rapidly in recent years.[1] Since the pioneering work of Afrosimov and co-workers on the T-4 and T-10 tokamaks[2] and Isler on the ISX-B tokamak,[3] this diagnostic tool has reached such a level of maturity that it is used routinely on several large tokamak facilities for measurements of impurity behavior[4-6] and plasma dynamical properties such as ion temperatures and toroidal rotation velocities.[7-12] The basic CXRS technique consists of measuring the intensity and/or spectral distribution of photons emitted in the charge exchange collision between fast neutral atoms and plasma ions:

$$H^{\circ} + A^{Z} \rightarrow H^{+} + (A^{Z-1})^{*} \qquad (1)$$

The product ion is left in an excited state which then radiatively decays to produce the observable photons. In Eq. (1) the neutral is denoted as hydrogen but other light atoms such as D° or Li° have also been used. These fast neutrals are provided by high energy neutral beam injection into the plasma, using either low power diagnostic beams or high power plasma heating beams. The most commonly observed product species are the hydrogenic ions produced from reactions with fully stripped low-Z impurity ions such as C^{6+} or O^{8+}, which are usually present in fusion plasmas.

The general advantages of CXRS over other passive spectroscopic techniques are: (1) the measurements are localized by the intersection volume between the neutral beamline and a collimated spectrometer sightline; (2) the emitted photons range in wavelength from the X-ray range all the way to the visible spectral range, where very simple remote optical systems can be used; (3) a single spectral line can be used for measurements across the entire plasma with the appropriate choice of elements; and (4) the photon emission rate resulting from reaction (1) is relatively independent of the local plasma environment (i.e., n_e, T_e, etc.) and depends only on the neutral beam characteristics and ion density in the intersection volume. The main disadvantages at present are: (1) a neutral beam is needed for most applications of CXRS and (2) some plasma environmental effects on the local emission rate and spectral line shape, although not of dominant influence, are not yet completely characterized.

We give here an overview of the use of CXRS as an active diagnostic tool for high temperature plasmas by concentrating on the following three applications of central importance to plasma research: (1) diagnosis of impurity densities and transport of ions across magnetic field lines; (2) the measurement of plasma dynamical properties such as ion temperatures and bulk rotation velocities; and (3) the measurement of the density and nonthermal velocity distribution of alpha particles produced in a fusion plasma. Other applications of CXRS such as spectrometer calibration,[13] atomic physics studies, beam attenuation studies, specialized diagnosis of edge plasma properties,[14] etc. are not discussed here in an effort to concentrate on the general applications of CXRS to plasma diagnosis. In the same spirit, we concentrate our discussion on the use of intrinsic, fully stripped, low-Z impurities such as C, O, and often He for such measurements, although similar measurements can of course be made with any other elements and/or ion species which may be present in (or actively injected into) a plasma.[15] When the bulk plasma ions consist of a single isotope such as H^+ or D^+, CXRS has also been used to measure the bulk ions themselves.[11,16] However, it is the low-Z elements, He, C, and O, which are most commonly present, and for which atomic cross sections and energy levels are very well characterized. Finally, we note that the discussion here revolves around the use of CXRS as a tokamak plasma diagnostic, but it can obviously be employed on other magnetic confinement devices. The experimental results presented here are exclusively from the PDX/PBX tokamak because we have ready access to this data, but we note that equivalent data have been produced by other groups and are referred to below.

II. IMPURITY DENSITY AND PARTICLE TRANSPORT MEASUREMENTS

In plasmas typical of those in present tokamak devices, C^{6+} and O^{8+} are the most abundant impurity species in the hot plasma core. Measurement of these ion densities and knowledge of their transport across the confining magnetic field are necessary for an evaluation of the performance of a variety of impurity control techniques. CXRS allows these densities to be measured directly instead of being inferred indirectly from measurements of lower charge states at the plasma periphery or estimates of the general plasma impurity levels. For impurity density or transport measurements it is desirable that the neutral beam be sufficiently low in power so that it does

not perturb the plasma or impurity ion species distribution. Very low beam powers and/or energies, however, will not provide enough penetration into the plasma core for good signal strength, so such beams will be most useful at lower plasma densities. Low signal levels on the PDX tokamak experiment were compensated for by square-wave modulation of the beam, allowing phase-locked detection of weak signals.[7] When high power heating beams are used for these measurements, the contributions to the signal from changing impurity distributions and plasma parameters due to the beam injection itself cannot be ignored. On ISX-B this is accounted for by switching between heating beams, only one of which is viewed by the spectrometer.[4]

A typical experimental setup for CXRS measurements of low-Z ion densities on the PDX tokamak is shown in Fig. 1. A highly collimated (FWHM ~ 3 cm) low power (~ 8-10 kW) diagnostic neutral beam (DNB) injects H^0 or D^0 across the plasma midplane. The neutral beam can be aimed at different locations in the plasma midplane on a shot-by-shot basis. A grazing incidence spectrometer was used to view the DNB, and the signal resulting from reaction (1) was verified to come from the small interaction volume defined by the intersection of the two beams by vertically scanning the spectrometer sightline over the beam.

An example of prompt charge-exchange-produced radiation from the experiment in Fig. 1 is shown in Fig. 2, in which the sharp pulses of O VIII 102Å (n = 3-2) emission are produced by the modulated DNB pulse. The beam-produced component in the overall signal is clearly seen above the background radiation which is produced by electron impact excitation of O^{7+} in the plasma periphery and charge exchange recombination of O^{8+} with the background thermal neutrals in the plasma.

The choice of which spectral line to observe with CXRS depends to a large degree on which measurements are desired and, less importantly, on available instrumentation. The charge exchange reaction (1) is a resonant process which populates a distribution of excited states with orbital and angular momentum quantum numbers n, ℓ. Theoretical partial cross sections $\sigma(n,\ell)$ for populating specific states are available from several authors.[17-19] In general, the total cross section for populating a given n level $\sigma(n) = \Sigma_\ell \sigma(n,\ell)$ peaks in n with $n_{max} \approx Z^{0.75}$. As the beam energy rises, the distribution of $\sigma(n)$ broadens in n and progressively higher states

are excited. The ℓ distribution is quite peaked at high ℓ for $n \leq n_{max}$ while it levels off or peaks at $\ell = n_{max}$ for $n > n_{max}$. Thus, the observed photons are produced in a complex cascade process which can obscure the original $\sigma(n, \ell)$ distribution. In practice, the fine structure is not observable in the transitions, and the total emission rate for a transition between states with different principal quantum number n is of interest. The $\Delta n = 1$ transitions are the most frequent and transitions between lowest n states will be brightest and least sensitive to uncertainties in the original electron distribution. This tends to make the short wavelength transitions between low n states most attractive for quantitative impurity measurements. As our knowledge of the $\sigma(n,\ell)$ distribution and possible plasma effects on the cascade process improve, the higher wavelength transitions between Rydberg states will become more attractive due to simpler instrumentation requirements.

The determination of impurity densities from signals such as in Fig. 2 involves several steps. First, an average beam-excited intensity is determined by simple measurement for strong signals or cross-correlation of the beam and spectrometer waveforms for weaker signals. The beam particle densities in the intersection volume must be calculated using standard beam attenuation codes using the measured plasma profiles as input.[20] Finally, cascade-corrected emission rates must be calculated for the transition and beam energies of interest. If the intersection volume is large, a model density profile may be necessary to integrate the emission rate over the intersection volume.

Impurity particle cross-field transport is conveniently modeled via the one-dimensional continuity equation for each ion species:

$$\frac{\partial n_q}{\partial t} + \frac{1}{r}\frac{\partial}{\partial r} r \left[-D(r)\frac{\partial}{\partial r} n_q + n_q v(r)\right] = -(I_q + R_q) n_q + I_{q-1} n_{q-1}$$

$$+ R_{q+1} n_{q+1} - \frac{n_q}{\tau_\parallel} + S_q \,. \qquad (2)$$

Here, n_q is the density of charge state q, D is a radial diffusion coefficient, v denotes a convective velocity for cross-field transport, I_q and R_q are the electron impact ionization and total recombination rates, respectively, $\tau_\parallel$ is a parallel particle loss time at the plasma edge and S_q is

a volume source for q = 1 from edge neutral particle influx. For simplicity, the radial flux is often modeled by a simple diffusive/convective term as in Eq. (2), and the problem is to determine the magnitude and functional forms of D(r) and v(r).

The particular virtue in using fully stripped, low-Z species for particle transport measurements lies in the fact that the time and spatial variations of $n_q(r,t)$ are determined mainly by transport processes, in contrast to the case of partially ionized higher-Z ions where the atomic processes on the right side of Eq. (2) dominate. Uncertainties in these atomic rates and/or basic plasma parameters have so far hindered efforts to derive detailed transport coefficients in fusion plasmas.[21]

Observations of the steady-state radial profiles of O^{8+} or C^{6+} on PDX were sufficient to show conclusively that these impurities are not in coronal equilibrium and that cross field transport must be considered.[5] Even for C and O, however, the atomic processes were important in PDX and steady-state profiles of C^{6+} and O^{8+} were insufficient to get accurate transport coefficients.

Since steady-state profiles of low-Z fully stripped ions allow only the ratio v(r)/D(r) to be determined, detailed measurements of particle transport involves introducing a source of impurities at the plasma edge and following them as they diffuse into the plasma. Such CXRS measurements with He^{++} were performed on PDX as an example of transport coefficient determination.[6] Figure 3 shows the measured time variation of the central He^{++} density following a puff of helium at the plasma edge using the apparatus in Fig. 1. Also shown are solutions to Eq. (2) for different values of D(r) = D (i.e., radially constant diffusion coefficient) with $v(r)/D \propto (\partial \ln n_e/\partial r)^{0.8}$, as derived from measurements of the steady-state radial profiles. The sensitivity of this relatively noisy data to distinguish different values of D and v is evident. Indeed, with measurements of $n_{He^{++}}(t)$ at several radii, it should be straightforwardly possible to measure the spatial dependence of the transport coefficients D(r) and v(r) for the first time with reasonable accuracy in tokamaks using CXRS. Once such measurements are made, comparison with more theoretically based transport models will be feasible.

III. PLASMA ION DYNAMICS

The most widespread and immediate use of CXRS has been the determination of plasma ion velocity distributions through measurement of spectral line shapes and positions. Since the charge exchange process does not involve any significant momentum exchange between the reactants, the spectral distribution of the emitted photons reflects the velocity distribution of the target ions A^Z in Eq. (1). This is, of course, strictly true only if the beam neutral velocity is much greater than the thermal velocity of the target ions (i.e., $v_B >> v_z$). Otherwise, the velocity dependence of the $\sigma(n,\ell)$'s must be considered. For thermalized ions in a reactor grade plasma, the condition $v_z << v_B$ is usually satisfied. Several measurements of plasma ion temperature using CXRS with H^+, He^{++}, or O^{8+} as the target species have verified that the derived values of $T_i(r)$ agree well with values obtained with conventional particle charge exchange and neutron measurements, and, in most cases, can probably be considered more accurate than those measurements. [9-11]

Since C and O occur naturally in most devices and their fully stripped ions occur at all radii due to cross field diffusion, a single ion and wavelength may be used to establish a radial profile. This is in contrast to the more conventional spectroscopic measurements which use a variety of impurity charge states to establish a radial profile of T_i (presupposing knowledge of the charge state radial distributions).

For spectral line profile measurements, one clearly desires to work with the longest possible wavelength emissions to ease instrumentation requirements on optical access, resolution, throughput, etc. Long wavelength lines originating from transitions between Rydberg states ($n > 4$) in hydrogenic spectra are excited by charge exchange, but the excitation rate coefficients decrease as n increases. An important feature for excitation of the longer wavelength lines is the need for high neutral particle energies. Even with such limitations, lines from He^+, C^{5+}, and O^{7+} in the near-UV to visible spectral ranges have all been observed with reasonable intensities for line profile measurements in several tokamaks. The low mass and high temperature of these ions results in easily measured line widths with standard moderate resolution spectrometers.

An especially attractive feature of measurements in the $\lambda > 3000$Å range is the ability to use radiation-hardened, fiber-optic imaging systems to

provide easy remote access to a reactor environment for ion velocity distribution measurements. This is a tremendously simplifying advantage of this technique over other approaches to T_i measurements. It offers flexibility for varied access to the machine and sophisticated imaging systems can be used to provide time-resolved radial profiles of ion temperature and bulk velocities in a single shot. When the beam energy is too low to sufficiently excite near-UV and visible spectral lines for fiber optic access, lines in the UV range (1000-3000Å) are sufficiently intense for reasonable measurements without extreme instrumentation requirements.

Assuming sufficient line intensities and good beam/spectrometer geometry, the major limitations to the CXRS technique for ion velocity distribution measurements arise from background light obscuring the desired signal and the possibility of nonthermal line broadening effects being present. Since all ions of an impurity species are present in the plasma, background radiation at the wavelengths of interest can be excited from the plasma periphery and fall in the spectrometer line of sight. Excitation via electron impact and/or charge exchange with thermal neutrals is most important for very low-Z ions such as He^{++}, but can also pollute measurements with O^{7+} at the plasma edge where the CXRS signal is also weak. If the neutral beam is not modulated to discriminate the signal excited by the beam in the intersection region, this radiation must be considered in the line profile analysis.

With very light ions such as He^{+}, the line broadening of the CXRS signal from the plasma interior is so much larger than the thermal broadening of the edge signal that a simple two-line model fitting procedure allows the CXRS signal to be isolated, as was done on D-III[9] and PDX.[10] With C^{5+} and O^{7+}, the background component comes from regions nearer the hot plasma core, and it is better to rely on observations in which the CXRS signal is much larger than the background signal to ensure a localized measurement. For O^{7+}, the electron excitation rates for high n transitions in O^{7+} and thermal neutral charge exchange with O^{8+} is so low that the charge-exchange-induced signal completely dominates when the interaction volume is in the plasma core region. At the plasma periphery, however, the reduced CXRS signal (due to decreasing n_z) and increased background signal (due to increasing n_{z-1} and increased thermal neutral density) conspire to make edge T_i measurements more

difficult using C^{5+} and O^{7+} in present machines with relatively low beam energies ($\lesssim$40 keV/amu).

All the above considerations, plus coincidental overlap with other plasma ion emission lines, tends to limit the number of transitions available for routine T_i measurements when the neutral beam is not modulated. In practice, the HeII 4686Å (4-3) and OVIII 2976Å (8-7) transitions are most commonly used on present machines.

An example of an experimental setup for CXRS measurements of T_i and v_ϕ in the PBX tokamak is shown in Fig.4.[22] A standard air-filled spectrometer with an optical multichannel detector views across a (perpendicular) heating neutral beam through a simple optical system. The rotating mirror allows a shot-by-shot spatial scan of $T_i(r,t)$ and $v_\phi(r,t)$. An optional fiber optic connection to another scanning mechanism allows optical access to one of the tangentially injected beamlines when only tangential injection is employed. The low beam energy of 22 keV/amu and lack of modulation precludes the use of any but the two spectral lines mentioned above for routine measurements.

A sample measurement of the time evolution of the OVIII 2976Å line intensity is shown in Fig. 5a. The intensity clearly is correlated with the turn-on of the NW beam and only a negligible background signal exists when the beam is off. In contrast, the OIII 2983.8Å line, which is excited by electron collisions at the plasma edge, is present throughout the discharge (Fig. 5b). Sample spectra early and late in the beam heated phase (Figs. 5c and d) show the large broadening and shift of the OVIII line, indicating increased plasma temperature and toroidal rotation speed at the plasma center. Meanwhile, the OIII line has hardly shifted at all, indicating the reduced rotation velocity at the plasma edge and coincidentally providing a convenient calibration wavelength.

The charge-exchange-excited-OVIII line is easily fitted with a gaussian profile to provide T_i and v_ϕ, and any non-Maxwellian features to the ion velocity distribution if present. Such a fit of a measured line to a gaussian is shown in Fig. 6a for a sample spectrum. Besides the usual correction due to the instrumental profile width (which is almost negligible here), the measured line width must also be corrected for possible broadening due to the spectral distribution of atomic fine structure components of the line. The intensity distribution of these components can vary depending on Zeeman and

motional Stark effects, beam energy, and collisional mixing, and a full calculation of such effects is exceedingly complex. However, since the thermal width is usually much broader than the fine structure splitting, only a crude approximation is needed to adjust the measured width to produce an accurate T_i. In Fig. 6b we show unperturbed field-free fine structure components as calculated for a 25 keV/amu beam. Comparison of the FWHM of the composite spectrum constructed by adding all fine structure contributions and the assumed T_i indicates that the measured T_i is ~ 3% less than inferred directly from the measured FWHM. The adjustment is usually small enough that only rough approximations are sufficient.

The time evolution of T_i and v_ϕ obtained from such analyses for a sample discharge in PBX are shown in Fig. 7. This technique is sufficiently sensitive that a time resolution of 4 ms in T_i measurements is readily achieved, and even higher time resolution appears feasible. A straightforward extension of such measurements to provide measurements at several spatial locations simultaneously allows radial profiles to be obtained in a single shot. Such a system has been employed on the D-III tokamak[23] and will be employed with a modulated neutral beam on the TFTR tokamak. With high spectral, time, and spatial resolution all required in a single shot, the data flow rate increases dramatically, which will lead to considerations of more sophisticated detector designs to minimize the amount of stored data.

IV. ALPHA PARTICLE DIAGNOSIS

The third major area of application of CXRS for diagnosis of fusion plasmas lies in the realm of measuring the densities and/or velocity distributions of alpha particles which are produced in a burning plasma. Significant densities of fusion-produced alphas ($n_\alpha \sim 10^{12}$ cm^{-3}) are expected in the present generation of large tokamaks such as TFTR and JET. The ability to measure properties of the confined alpha distribution is necessary to study the behavior and confinement of these particles in an ignited plasma. In addition, the ability to measure fusion ash products (i.e., He^{++} in the core plasma) allows the evaluation of such devices as magnetic divertors and particle scoop limiters for controlling ash buildup in a burning plasma.

Measurements of thermalized He^{++} via CXRS have already been demonstrated on PDX (c.f. Fig. 3 and Ref. 6), but the measurement of the fast (i.e.,

unthermalized) alpha particles entails operating in a different velocity regime than usual for CXRS. In this case, the alpha particles have speeds much greater than that of the typical neutral beam atom (i.e., $v_\alpha >> v_B$), and the velocity dependence of the cross sections cannot be ignored.

Post and co-workers have developed several concepts for using charge exchange to detect and study fast alphas.[24] Their basic idea takes advantage of the resonant character of the charge exchange process by noting that the cross sections for charge exchange fall rapidly above a relative cutoff speed denoted by $v_c \approx 2\text{-}3 \times 10^8$ cm/s. If a very high energy beam is used, only particles with $|\vec{v}_B - \vec{v}_\alpha| \lesssim v_c$ undergo charge exchange reactions with subsequent photon decay, thus allowing one to sample regions of the alpha velocity phase space distribution (Fig. 8a). The resulting spectrum emitted by the fast recombined He^+ depends strongly on the slowing down distribution of the alphas and allows a discrimination between classical and nonclassical fast alpha loss processes. The charge exchange excited line shape will be shifted roughly by $v_\parallel/c$ where $v_\parallel$ denotes the speed of the beam particles along the spectrometer line of sight, and it will be broadened by a width corresponding to a speed of $\sim v_c$.

Figure 8b shows a conceptual experimental approach to sampling the α distribution near the birthing energy of 0.88 MeV/amu by viewing the shifted and broadened spectrum of the 304Å (2-1) transition in He^+. The choice of transition to observe is limited by practical and atomic physics considerations. The n = 4 state He^+ is subject to substantial proton-impact ionization for fast He^+ ions and hence the photon emission rate from that transition will be suppressed. Also, the partial cross sections for population of a given n level in He^+ due to charge exchange reactions of a neutral atom with He^{++} peaks at $n \approx 2$ and 3 for H° and Li° neutrals, respectively. The n = 2-1 transition at 304Å is not very favorable due to strong impurity emission lines in that region and the need to use grazing incidence optics there. Since estimates of the expected signal strengths are very low for $n_\alpha \sim 10^{12}$ cm^{-3}, high optical throughput is required to get good statistics and allow discrimination from the background bremsstrahlung continuum radiation. Hence, the n = 3-2 transition at 1640Å appears to be the best candidate for alpha diagnosis using CXRS. In addition, since Li° beams will preferentially populate the n = 3 level in He^+, a multi-MeV Li neutral

beam is the best choice for detailed measurements of the fast-alpha distribution. The time and expense involved in developing such high energy beams appear to be high.

Substantial progress can be made by using available H° or D° beam systems on present tokamaks. For example, the diagnostic neutral beam system on the TFTR tokamak (P_{INJ} = 700 kW, E_o = 80 keV H° or D°)[25] has sufficient energy to sample far enough into the alpha velocity distribution to allow one to determine if the slowing-down energy spectrum is highly nonclassical or not. A very crude idea of the expected spectrum around the He^+ 1640Å line with the TFTR DNB used as a doping beam for CXRS is shown in Fig. 9 for a typical Q = 1 model plasma. Two distributions are shown, one assuming a classical slowing-down spectrum for the alphas, the other assuming that a non-classical loss process produces an anomalous loss of fast alphas during their slowing-down process, which results in a depleted velocity distribution at low velocities.[24] The profiles shown in Fig. 9 were constructed using the calculated rate coefficients and spectral line shift from Ref. 28. The profile of the line is taken to be gaussian with a FWHM corresponding to $v \sim v_c$. Contributions from all three beam energy species (i.e., E_o, $E_o/2$, $E_o/3$) are included. We have not included estimates of either the narrow width background signal at $\Delta\lambda = 0$ due to edge recycling of thermal He^{++} or the broad component arising from charge exchange excitation of the thermal He^{++} in the plasma core. Finally, the continuum bremsstrahlung emission level is also indicated in Fig. 9. We see that the expected CXRS signal from the fast alphas is comparable to the continuum level. Such a signal should be detectable with a high contrast spectrometer with large optical throughput to achieve sufficient statistics, and the difference between a classical and strongly nonclassical slowing-down process should be evident. For measurements of the alpha distribution in TFTR to be successful, modulation of the neutral beam is necessary to eliminate the background signals due to edge recycling and continuum radiation, and square wave modulation up to a few kHz is planned.

V. PLASMA ENVIRONMENTAL EFFECTS

The charge exchange and subsequent radiative decay processes are also influenced by the surrounding plasma environment. Without significant mixing

among different ℓ levels, the selection rules $\Delta\ell = \pm 1$ holds rigorously during the cascade process. If, however, significant mixing occurs, the cascade process can differ considerably from that expected in a field-free environment. Detailed calculations of such effects are quite complex, and simple approximations are usually made to estimate the degree of level mixing. Zeeman and motional Stark effects can cause mixing among the fine structure levels in a given excited state and perturb the radiation pattern from that expected by field-free calculations of the partial cross sections $\sigma(n,\ell)$. Mixing of states by coupling $\Delta j = o$ levels occurs due to the motional Stark and plasma microfields, and Zeeman mixing of $\Delta j = 1$ levels can occur, especially among levels with high j.[1,10]

An important mixing process which can occur in reasonably high density plasmas is the collisional mixing among fine structure levels due to ion-ion impact. The principal quantum level n at which significant collisional mixing occurs for a given plasma density is indicated in Fig. 11, where we plot the results from two analyses for the onset of ℓ mixing. For either curve, one calculates the value of the ordinate for given plasma conditions. If the value of the ordinate lies above the corresponding curve for a given n state, collisional ℓ mixing can be ignored, while it is of increasing importance as the value falls below the curve.

The solid line in Fig. 10 indicates collisional mixing criteria developed by Pengelly and Seaton and extrapolated to fusion plasma parameters in Ref. 10. They simply require that the ℓ-averaged value of $A_{n\ell}\ \tau^c_{n\ell}$ be greater than 1, where $A_{n\ell}$ is the spontaneous emission rate from level $n\ell$ to lower level and $\tau^c_{n\ell}$ is the ion-ion collisional lifetime of level $n\ell$ for transfer to levels $n\ell\pm1$. This is a relatively soft criterion that indicates when ℓ mixing is important among high-ℓ levels. The dotted line, on the other hand, denotes estimates by Sampson for the condition of complete statistical mixing derived by demanding that $A_{nj}\ \tau^c_{nj} > 1$ for all levels nj (where $j = \ell\pm1/2$).[26] Since the np levels are strongly coupled to the ground state, this criterion is considerally more stringent than the first. It denotes the extreme plasma density above which a statistical distribution among excited levels must be assumed during the cascade process. Significant changes in the total emission rates occur if complete mixing occurs.

As an example, for $n_e = 3 \times 10^{13} cm^{-3}$, He^+ levels are completely mixed

for $n \gtrsim 3$ while O^{7+} is fully mixed for $n \gtrsim 10$, although significant mixing among higher ℓ levels may occur for $n \gtrsim 6$. Thus, while collisional mixing will be important in alpha particle diagnostics, the calculated rate coefficients for C^{5+} and O^{7+} $\Delta n = 1$ transitions are reasonably accurate for impurity measurements. Mixing among higher-ℓ levels can, however, affect the fine structure correction to ion temperature measurements. Fortunately, these corrections vary by only 5% or so whether no or full mixing is assumed. Level mixing should be most evident in the relative intensities of $\Delta n > 2$ transitions, which are so far of little plasma diagnostic interest.

In addition to the aforementioned intrinsic background radiation near a spectral line of interest, another source of nonlocalized radiation in the spectrometer line of sight at the same wavelengths as those of interest arises from electron-impact excitation of hydrogenic ions created along the neutral beam but outside the beam/spectrometer intersection region. These recombined ions form a plume which drifts along the magnetic field lines and can emit radiation in the plasma outside the intersection volume before ionizing. This ion plume effect is most severe for very light ions such as He^+, whose electron impact excitation rates are high.[10] It is also most important at low beam energies when the charge exchange excitation rate for the higher Rydberg transitions is very low but the total charge exchange rate is high. In both of these cases, appropriate choice of beam/spectrometer geometry minimizes these effects.

VI. CONCLUSIONS

Charge exchange recombination spectroscopy clearly provides a very versatile active diagnostic tool to probe the properties of high temperature plasmas. Its simplicity and modest instrumentation requirements have made it become a standard technique for ion temperature measurements in most major tokamak facilities. Despite its versatility, it does have limitations due mostly to the desire to use long wavelength transitions for these measurements. It is just the high-n Rydberg transitions of interest which require high beam energies for large excitation rates and which are most prone to be perturbed by the surrounding plasma environment. However, the ability to use fiber optic coupling and/or sophisticated optical imaging systems at long wavelengths is a tremendous advantage of this technique over other

spectroscopic diagnostic techniques.

Future development of CXRS as a high temperature plasma diagnostic will inevitably proceed in several directions. Further refinements of the excitation rates for long wavelength transitions should allow these transitions to be used for absolute impurity density measurements. Increasingly sophisticated instrumentation involving imaging detectors, modulated diagnostic neutral beams, high throughput moderate resolution spectrometers, etc. are all being developed for present and future fusion devices. Experimental applications of CXRS to spectrometer calibrations, atomic rate coefficient determinations, neutral beam attenuation measurements, atomic physics studies of charge exchange with higher-Z ions, etc. will also continue to mature in the near future.

The measurement of fusion-produced alpha particles is one of the most challenging yet most important future applications of CXRS in fusion research. Operation in the qualitatively new physics regime where $v_\alpha > v_B$ will require an increased level of sophistication in both data acquisition and analysis procedures. However, such a diagnostic will be necessary to study the production of alphas expected in the present generation of large tokamak experiments.

ACKNOWLEDGMENTS

Much of the work described here was done in collaboration with K. Jaehnig of PPPL. The uthor wishes to thank R. Hulse, R. Isler, R. Groebner, and D. Post for useful discussions. R. Goldston and H. Towner provided invaluable aid in the beam attenuation code development, while P. Roney and E. Powell has assisted in the software development on the PDX and PBX tokamaks. This work was supported by U.S. Dept. of Energy Contract No. DE-AC02-76-CHO-3073.

REFERENCES

1 R. C. Isler, to be published in the Proceedings of the International Conference on the Physics of Highly Ionized Atoms, Oxford, July 2-5, 1984.

2 V. V. Afosimov, Yu. S. Gordeev, A. N. Zimov'ev, and A. A. Korothov, Sov. J. Plasma Phys. 5, 551 (1979); A. N. Zimov'en, A. A. Korthov, E. R. Krzhizhanovshii, V. V. Afosimov, and Yu. S. Gordeev, JETP Lett. 32, 539 (1980).

3 R. C. Isler, Phys. Rev. Lett. 38, 1359 (1977).

4 R. C. Isler et al., Phys. Rev. A 24, 2701 (1981).

5 R. J. Fonck, M. Finkenthal, R. J. Goldston, D. L. Herndon, R. A. Hulse, R. Kaita and D. D. Meyerhofer, Phys. Rev. Lett. 49, 737 (1982).

6 R. J. Fonck and R. A. Hulse, Phys. Rev. Lett. 52, 530 (1984).

7 R. J. Fonck, R. J. Goldston, R. Kaita, and D. Post, Appl. Phys. Lett. 42, 239 (1983).

8 R. C. Isler and L. E. Murray, Appl. Phys. Lett. 42, 355 (1983).

9 R. J. Groebner, N. Brooks, K. Burrell, and L. Rottler, Appl. Phys. Lett. 43, 920 (1983).

10 R. J. Fonck, D. S. Darrow, and K. P. Jaehnig, Phys. Rev. A 29, 3288 (1984).

11 G. A. Cottrell, Nucl. Fusion 23, 1689 (1983).

12 S. Suckewer, C. H. Skinner, B. Stratton, R. Bell, A. Cavallo, J. Hosea, D. Hwang, and G. Schilling, Appl. Phys. Lett. 45, 236 (1984).

13 R. C. Isler and R. A. Langley, to be submitted for publication.

14 H. Winter, Comm. At. Mol. Phys. 12, 165 (1982).

15 C. H. Skinner. S. Suckewer, S. A. Cohen, G. Schilling, and R. Wilson, Phys. Rev. Lett. 53, 458 (1984).

16 E. L. Berzovsky, M. M. Berezovskaja, A. B. Kzvozchikov, V. A. Krupin, and V. A. Ronstev - Kartinov, to be published.

17 R. E. Olson, in Electronic and Atomic Collisions, edited by N. Oda and K Takayunagi (North-Holland, Amsterdam, 1980).

18 E. J. Shipsey, T. A. Green, and J. C. Browne, Phys. Rev. A 27, 821 (1983); T. A. Green, E. J. Shipsey, and J. C. Browne, Phys. Rev. A 25, 1364 (1982).

19 H. Ryufuku, Japan Atomic Energy Research Institute Report JAERI-82-031, 1982. (unpublished).

20 R. J. Goldston, D. C. McCune, H. H. Towner, S. L. Davis, R. J. Hawryluk, and G. L. Schmidt, J. Comput. Phys. 43, 61 (1981).

21 R. A. Hulse and R. J. Fonck, Bull. Am. Phys. Soc. 28, 1153 (1983).

22 K. P. Jaehnig, R. J. Fonck, K. Ida, and E. Powell, Princeton Plasma Physics Report PPPL-2172 (1984), to be published in Rev. Sci. Instrum.

23 R. P. Seraydarian, K. H. Burrell, N. H. Brooks, R. J. Groebner, and C. Kahn, Bull. Am. Phys. Soc. 28, 1102 (1983).

24 D. E. Post, D. R. Mikkelson, R. A. Hulse, L. D. Stewart, and J. C. Weisheit, J. Fusion Energy 1, 129 (1981).

25 S. S. Medley, R. J. Goldston, and H. H. Towner, Princeton Plasma Physics Report PPPL-1673 (1980), unpublished.

26 D. H. Sampson, J. Phys. B 10, 749 (1979).

FIGURE CAPTIONS

FIG. 1 Experimental apparatus for charge exchange recombination spectroscopy on the PDX tokamak. (From Ref. 5)

FIG. 2 Excitation of O VIII 102Å (n = 3 → 2) emission by charge exchange induced by the pulsed diagnostic neutral beam in Fig. 1. (From Ref. 5).

FIG. 3 (a) Time evolution of near-central He^{++} density in the PDX tokamak after a short helium gas puff at the plasma edge.
(b) Change in the central chord He^{+} 304Å radiation at the plasma edge. The He^{++} density was measured with the apparatus in Fig. 1. The solid and dashed lines in (a) represent solutions to the coupled transport equations [Eq. (2) in the text] with $v(r)/D = 0.8\ \partial(\ln ne)/\partial r$. (From Ref. 6).

FIG. 4 Experimental arrangement for ion temperature measurements in the PBX tokamak using CXRS.

FIG. 5 Spectral signals from the PBX tokamak during neutral beam injection. (a) Time evolution of the charge-exchange-induced signal of O VIII 2976Å (7-6) emissions, showing the sharp increase in intensity when the northwest beam is on. (b) Behavior of the edge O III 2983Å intensity which is excited by electron collisions throughout the discharge duration. (c) Spectrum in the 2980Å range at t = 400 - 420 ms, just after the NW beam turns on. (d) Spectrum at t = 660 ms, showing the shifted and broadened charge-exchange signal.

FIG. 6 (a) Gaussian fit to a single line profile (Δt = 20 ms) of O VIII 2976Å obtained on PBX. (b) Relative intensities of the field-free fine structure components for excitation by 25 keV/amu neutrals.

FIG. 7 Time evolution of the central ion temperature and rotation velocity in PBX obtained via CXRS.

FIG. 8 (a) Schematic of alpha particle velocity space, wherein the large circle represents $v_{\alpha f}$ the edge of the alpha-particle distribution, and the small circle indicates the relative size of v_c. (b) Schematic diagram of CXRS experimental arrangement for measuring the fast alpha distribution. [(a) from Ref. 28].

FIG. 9 Rough estimates of the expected CXRS signal in TFTR using a 40 keV/amu D° diagnostic beam in a $Q = 1$ plasma. (a) Expected spectral distribution assuming classical slowing-down processes. (b) Spectrum calculated assuming a nonclassical distribution which is heavily depleted for $v \lesssim 8 \times 10^8$ cm/sec. The bremsstrahlung continuum intensity is also noted in (a).

FIG. 10 Estimates of critical n value for onset of fine structure level mixing due to plasma-ion collisions. The solid line represents estimates for the onset of mixing among the higher-ℓ levels, while the dashed line represents the condition for complete statistical mixing among all levels. N_e is in units of 10^{13} cm^{-3}, T_i in keV, and Z is the nuclear charge of the hydrogenic ion.

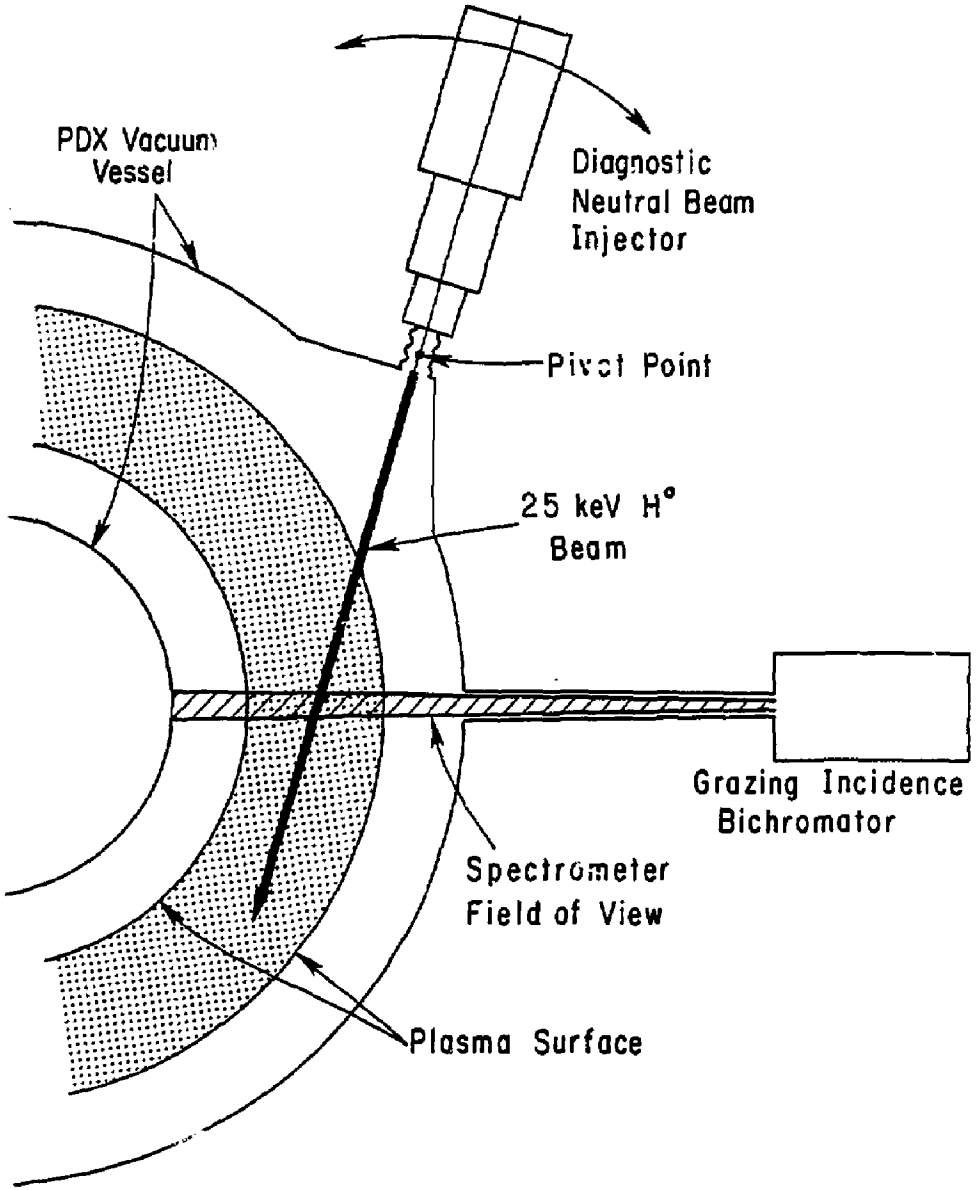
PDX Vacuum Vessel
Diagnostic Neutral Beam Injector
Pivot Point
25 keV H° Beam
Grazing Incidence Bichromator
Spectrometer Field of View
Plasma Surface

Figure 1

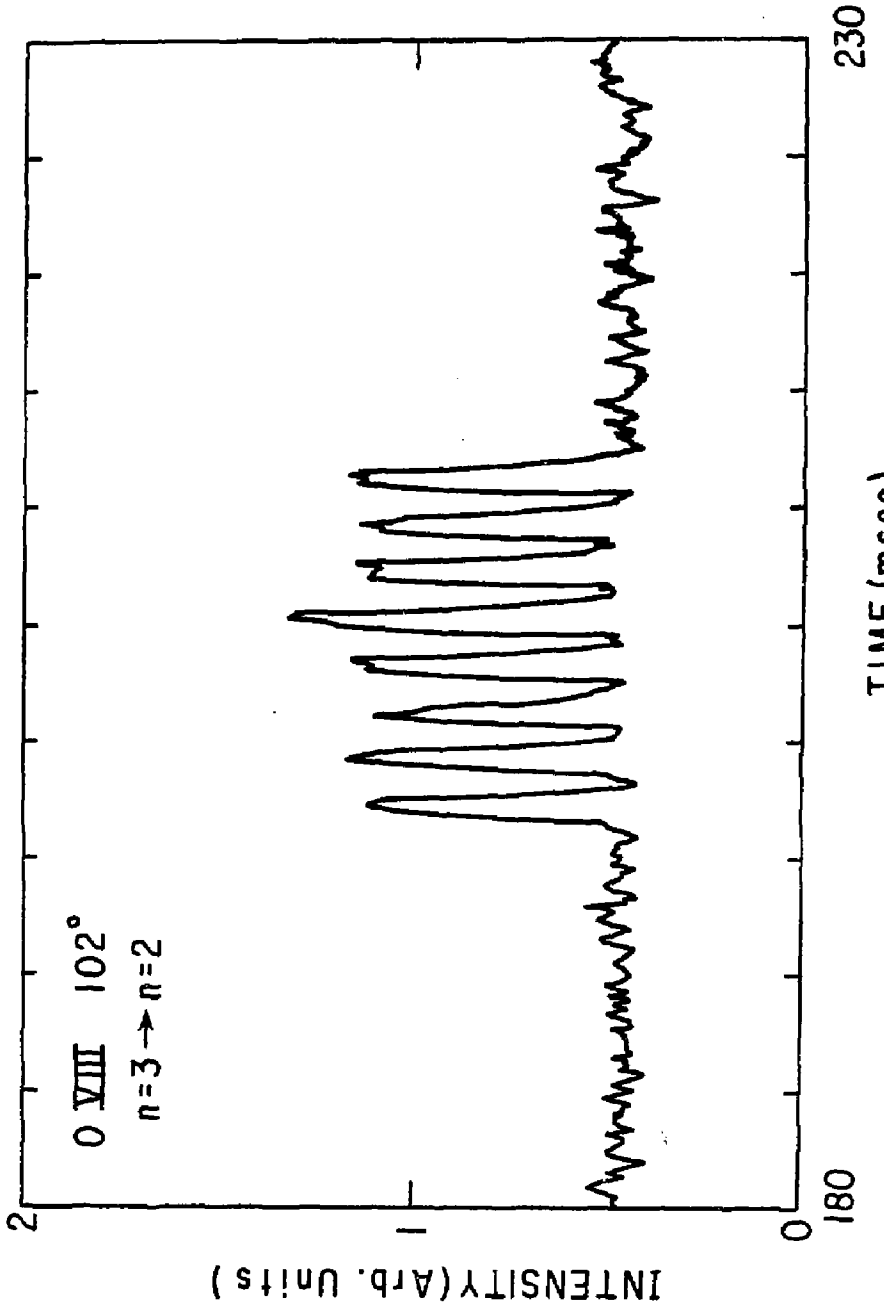
#82X0248
O VIII 102°
n=3→n=2
INTENSITY (Arb. Units)
TIME (msec)
2
1
0
180
230

Figure 2

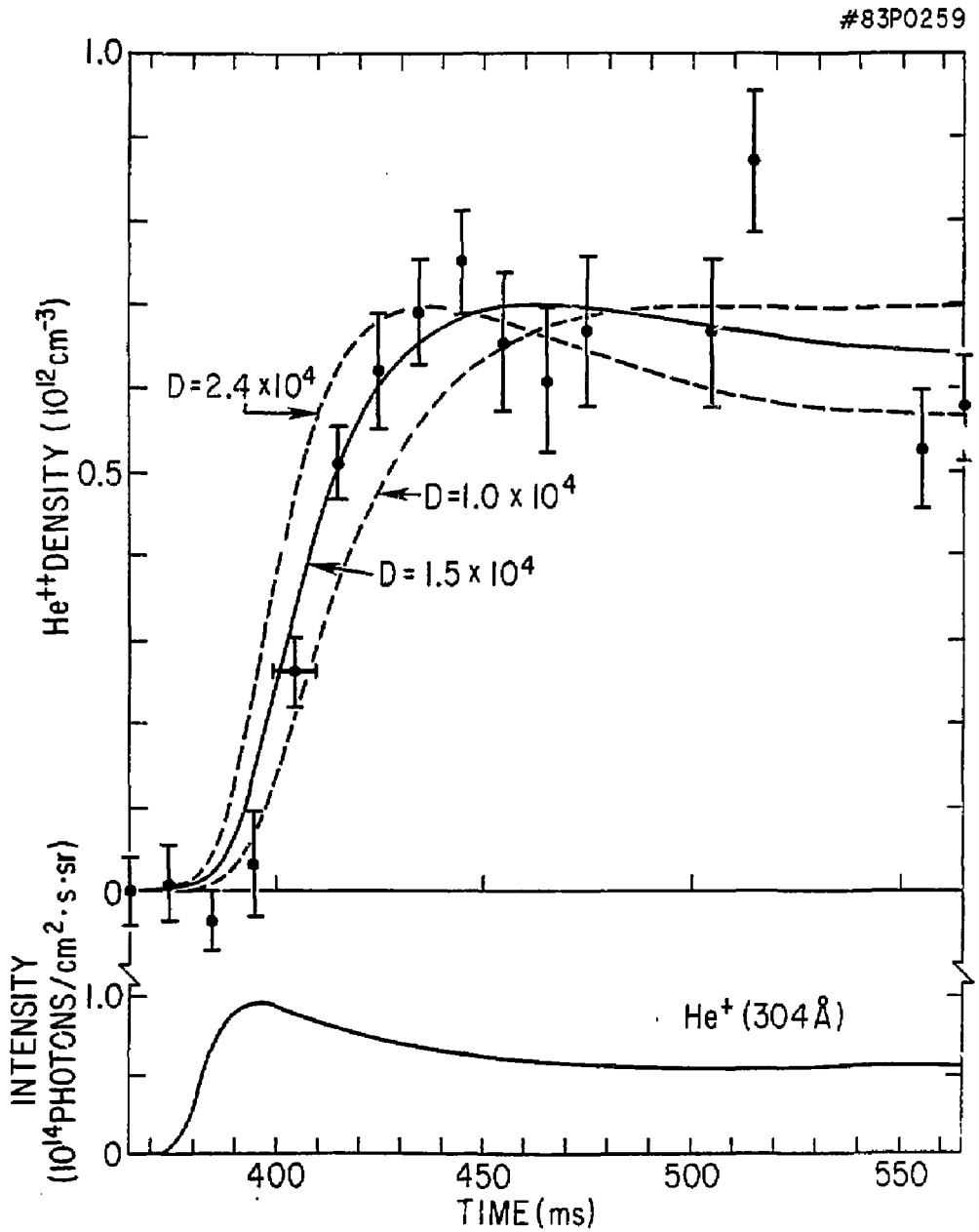
#83P0259
1.0
0.5
0
He++DENSITY (10^12 cm^-3)
D=2.4 x10^4
D=1.0 x 10^4
D = 1.5 x 10^4
INTENSITY
(10^14 PHOTONS/cm^2 · s · sr)
1.0
0
He+ (304 Å)
400
450
500
550
TIME (ms)

Figure 3

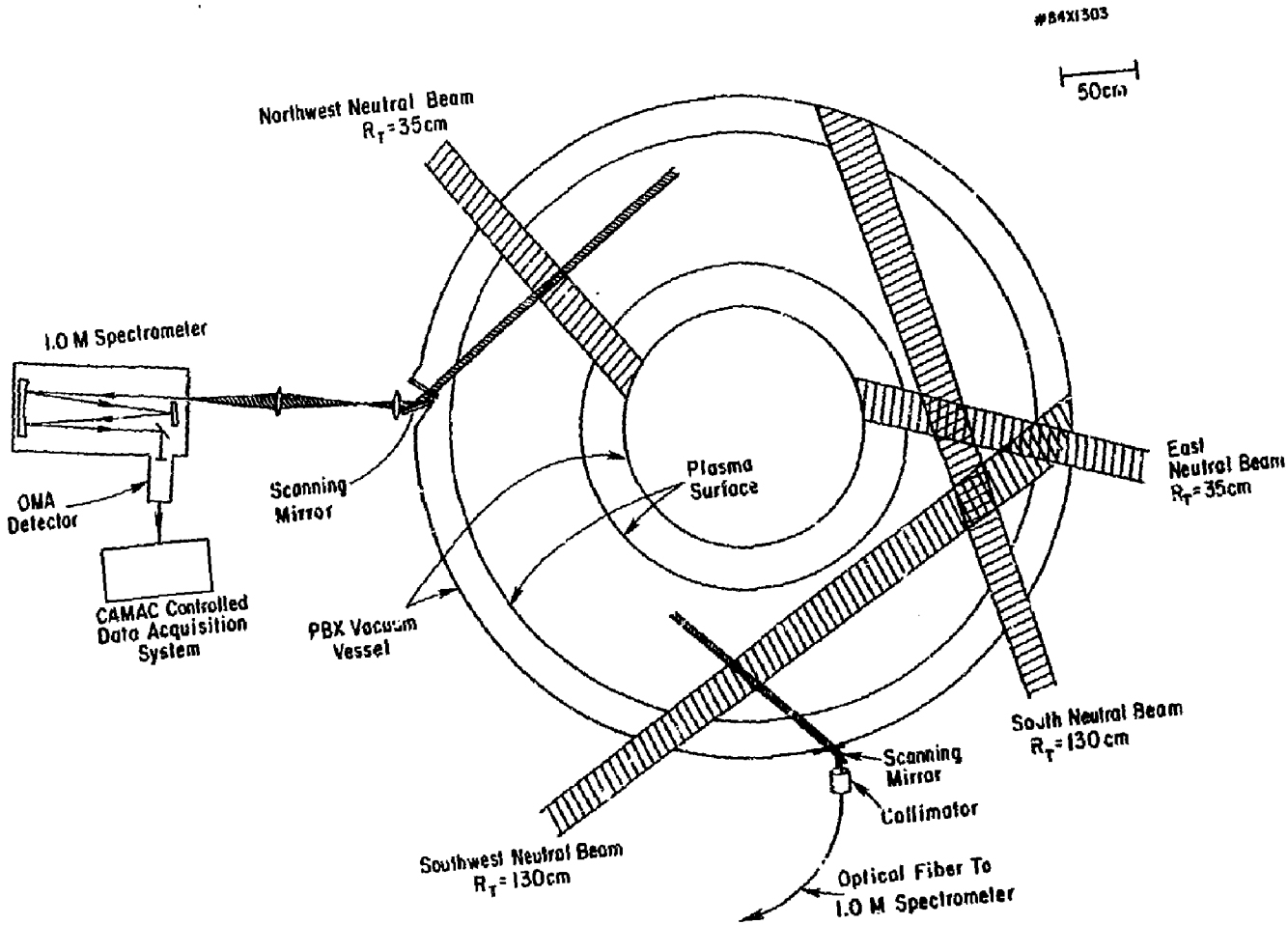
#84X1303
50cm
Northwest Neutral Beam
R_T=35cm
1.0 M Spectrometer
OMA
Detector
CAMAC Controlled
Data Acquisition
System
Scanning
Mirror
PBX Vacuum
Vessel
Plasma
Surface
East
Neutral Beam
R_T=35cm
South Neutral Beam
R_T=130cm
Scanning
Mirror
Collimator
Southwest Neutral Beam
R_T=130cm
Optical Fiber To
1.0 M Spectrometer

Figure 4

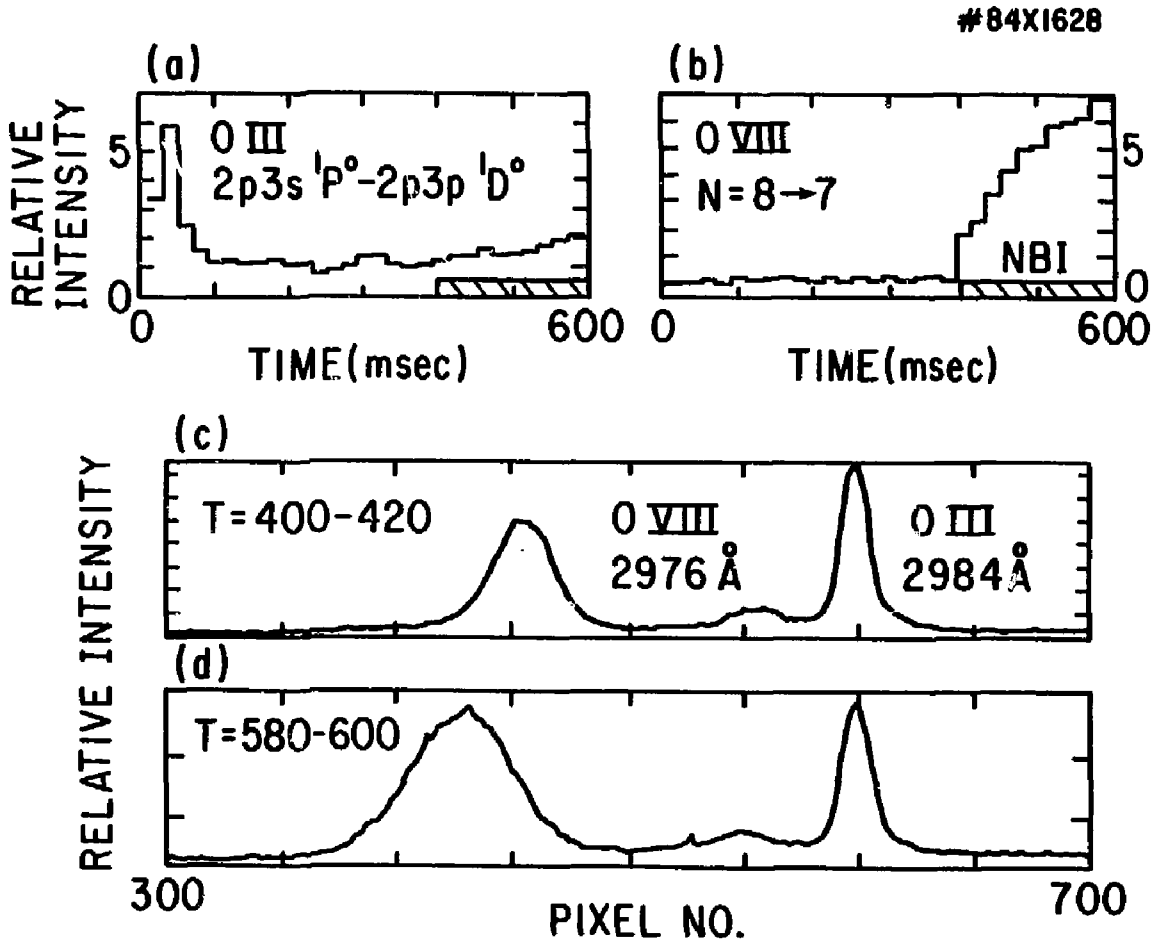
#84X1628
(a)
O III
2p3s ¹P°-2p3p ¹D°
RELATIVE INTENSITY
5
0
0
600
TIME(msec)
(b)
O VIII
N=8→7
NBI
5
0
0
600
TIME(msec)
(c)
T=400-420
O VIII
2976 Å
O III
2984 Å
(d)
T=580-600
RELATIVE INTENSITY
300
700
PIXEL NO.

Figure 5

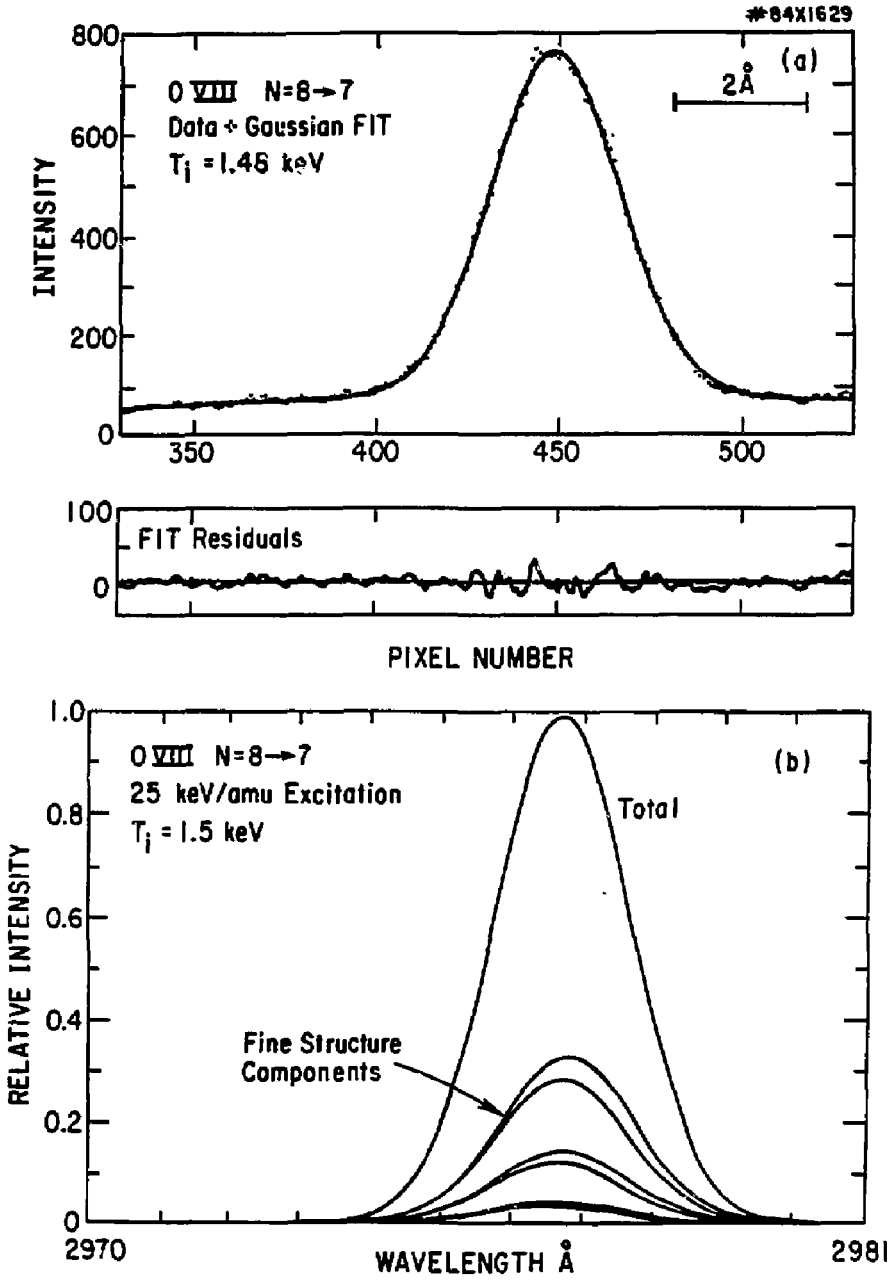
#84X1629
(a)
O VIII N=8→7
Data ÷ Gaussian FIT
T_i = 1.48 keV
2Å
INTENSITY
800
600
400
200
0
350
400
450
500
100
FIT Residuals
0
PIXEL NUMBER
(b)
O VIII N=8→7
25 keV/amu Excitation
T_i = 1.5 keV
Total
Fine Structure Components
RELATIVE INTENSITY
1.0
0.8
0.6
0.4
0.2
0
2970
WAVELENGTH Å
2981

Figure 6

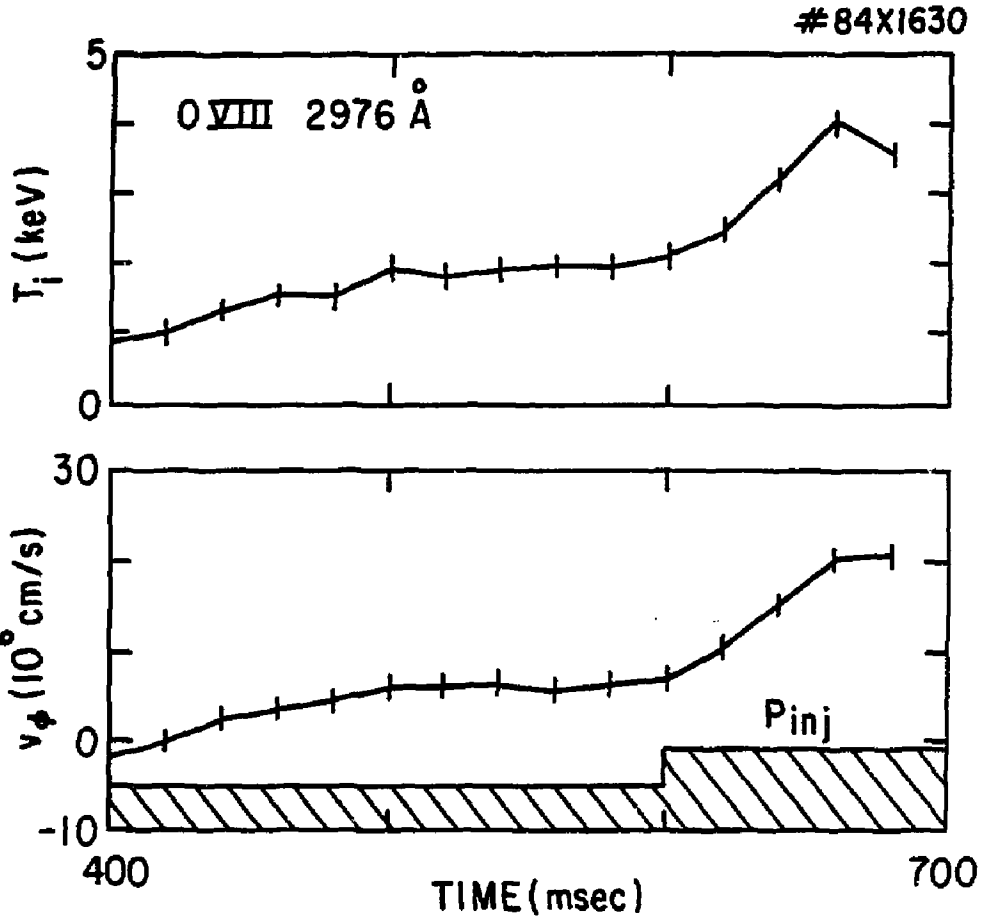
#84X1630
5
O VIII 2976 Å
T_i (keV)
0
30
v_ϕ (10^6 cm/s)
0
-10
P_{inj}
400
TIME (msec)
700

Figure 7

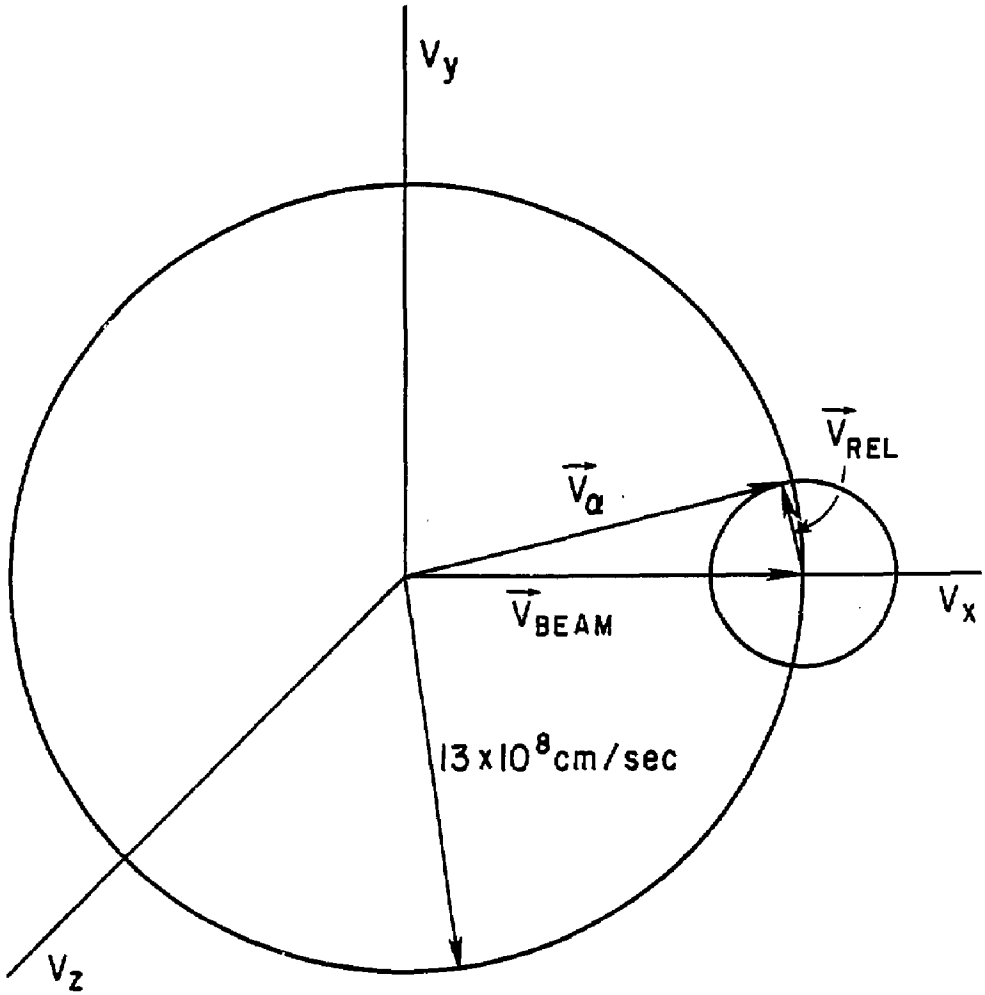

Figure 8a

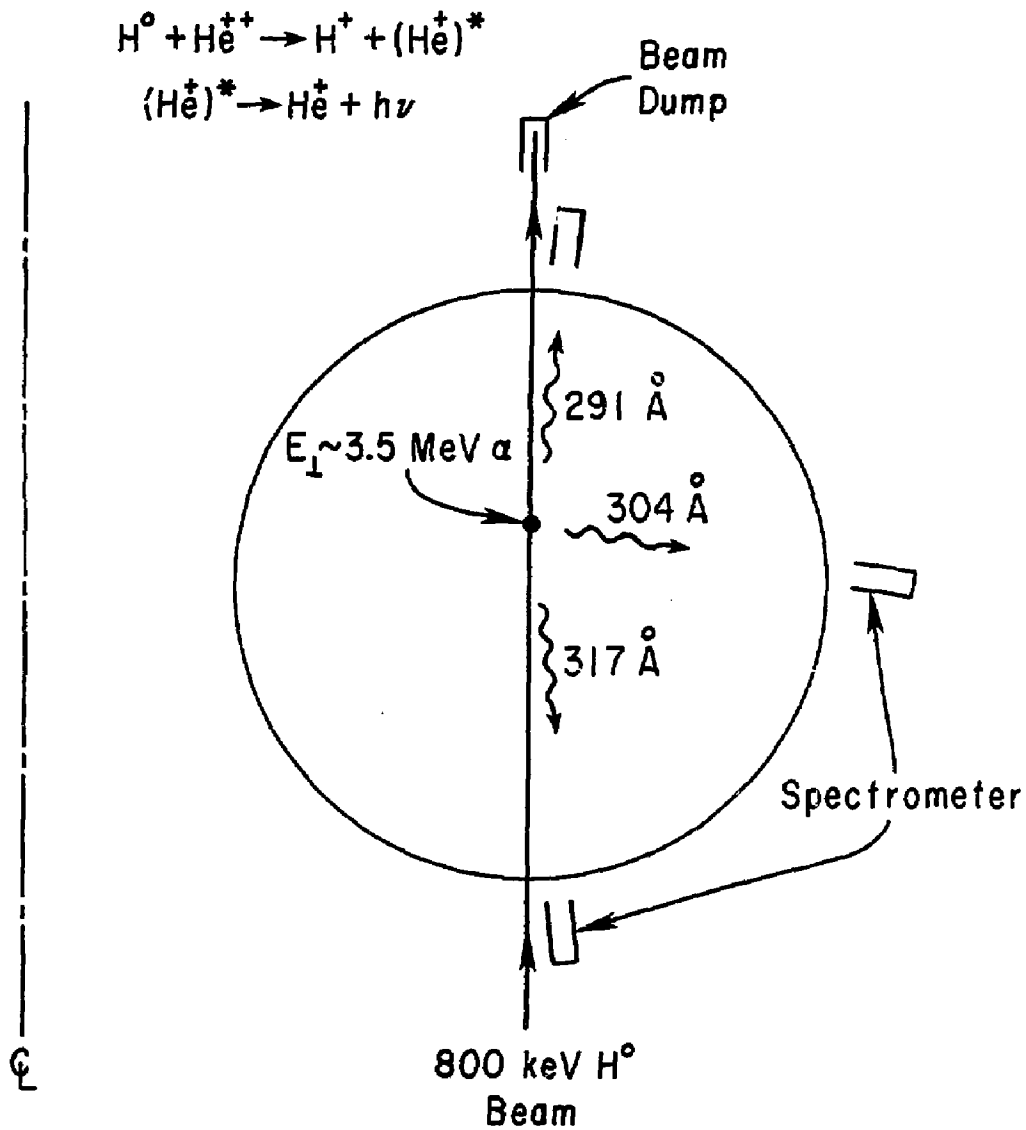
$H^0 + He^{++} \rightarrow H^+ + (He^+)^*$
$(He^+)^* \rightarrow He^+ + h\nu$
Beam
Dump
291 Å
$E_\alpha \sim 3.5$ MeV α
304 Å
317 Å
Spectrometer
800 keV H°
Beam

Figure 8b

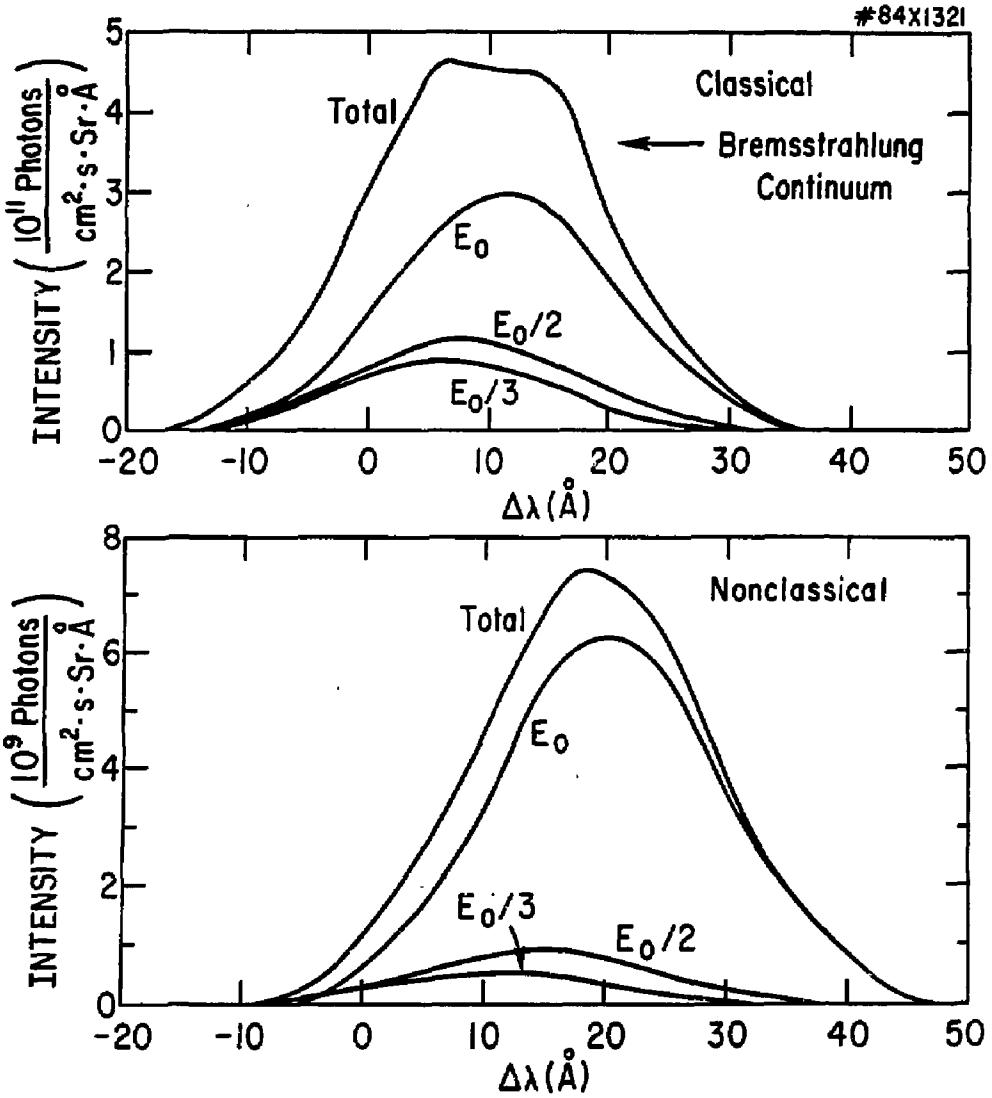
#84X1321
Classical
Total
Bremsstrahlung
Continuum
E_0
$E_0/2$
$E_0/3$
INTENSITY $\left(\frac{10^{11}\ \text{Photons}}{\text{cm}^2 \cdot \text{s} \cdot \text{Sr} \cdot \text{Å}}\right)$
$\Delta\lambda$(Å)
Nonclassical
Total
E_0
$E_0/3$
$E_0/2$
INTENSITY $\left(\frac{10^{9}\ \text{Photons}}{\text{cm}^2 \cdot \text{s} \cdot \text{Sr} \cdot \text{Å}}\right)$
$\Delta\lambda$(Å)

Figure 9

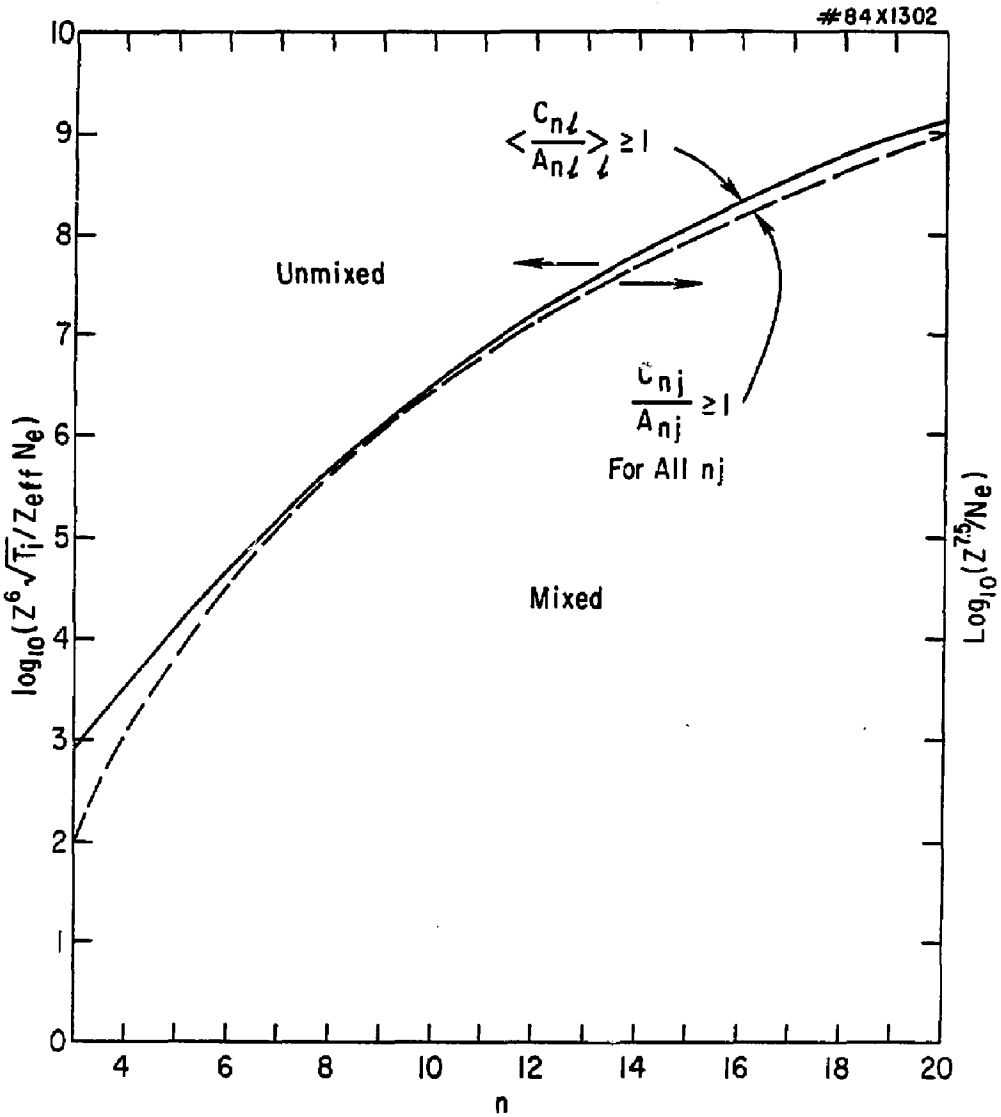
#84X1302
$\left\langle \frac{C_{n\ell}}{A_{n\ell}} \right\rangle_\ell \geq 1$
Unmixed
$\frac{C_{nj}}{A_{nj}} \geq 1$
For All nj
Mixed
$\log_{10}(Z^6\sqrt{T_i}/Z_{eff}\,N_e)$
$\mathrm{Log}_{10}(Z^{7.5}/N_e)$
n
0
1
2
3
4
5
6
7
8
9
10
4
6
8
10
12
14
16
18
20

Figure 10

EXTERNAL DISTRIBUTION IN ADDITION TO TIC UC-20

Plasma Res Lab, Austra Nat'l Univ, AUSTRALIA
Dr. Frank J. Paoloni, Univ of Wollongong, AUSTRALIA
Prof. I.R. Jones, Flinders Univ., AUSTRALIA
Prof. M.H. Brennan, Univ Sydney, AUSTRALIA
Prof. F. Cap, Inst Theo Phys, AUSTRIA
Prof. Frank Verheest, Inst theoretische, BELGIUM
Dr. D. Palumbo, Dg XII Fusion Prog, BELGIUM
Ecole Royale Militaire, Lab de Phys Plasmas, BELGIUM
Dr. P.H. Sakanaka, Univ Estadual, BRAZIL
Dr. C.R. James, Univ of Alberta, CANADA
Prof. J. Teichmann, Univ of Montreal, CANADA
Dr. H.M. Skarsgard, Univ of Saskatchewan, CANADA
Prof. S.R. Sreenivasan, University of Calgary, CANADA
Prof. Tudor W. Johnston, INRS-Energie, CANADA
Dr. Hannes Barnard, Univ British Columbia, CANADA
Dr. M.P. Bachynski, MPB Technologies, Inc., CANADA
Zhengwu Li, SW Inst Physics, CHINA
Library, Tsing Hua University, CHINA
Librarian, Institute of Physics, CHINA
Inst Plasma Phys, Academia Sinica, CHINA
Dr. Peter Lukac, Komanskeho Univ, CZECHOSLOVAKIA
The Librarian, Culham Laboratory, ENGLAND
Prof. Schatzman, Observatoire de Nice, FRANCE
J. Radet, CEN-BP6, FRANCE
AM Dupas Library, AM Dupas Library, FRANCE
Dr. Tom Mual, Academy Bibliographic, HONG KONG
Preprint Library, Cent Res Inst Phys, HUNGARY
Dr. S.K. Trehan, Panjab University, INDIA
Dr. Indra, Mohan Lal Das, Banaras Hindu Univ, INDIA
Dr. L.K. Chavda, South Gujarat Univ, INDIA
Dr. R.K. Chhajlani, Var Ruchi Marg, INDIA
P. Kaw, Physical Research Lab, INDIA
Dr. Phillip Rosenau, Israel Inst Tech, ISRAEL
Prof. S. Cuperman, Tel Aviv University, ISRAEL
Prof. G. Rostagni, Univ Di Padova, ITALY
Librarian, Int'l Ctr Theo Phys, ITALY
Miss Clelia De Palo, Assoc EURATOM-CNEN, ITALY
Biblioteca, del CNR EURATOM, ITALY
Dr. H. Yamato, Toshiba Res & Dev, JAPAN
Prof. M. Yoshikawa, JAERI, Tokai Res Est, JAPAN
Prof. T. Uchida, University of Tokyo, JAPAN
Research Info Center, Nagoya University, JAPAN
Prof. Kyoji Nishikawa, Univ of Hiroshima, JAPAN
Prof. Sigeru Mori, JAERI, JAPAN
Library, Kyoto University, JAPAN
Prof. Ichiro Kawakami, Nihon Univ, JAPAN
Prof. Satoshi Itoh, Kyushu University, JAPAN
Tech Info Division, Korea Atomic Energy, KOREA
Dr. R. England, Ciudad Universitaria, MEXICO
Bibliotheek, Fom-Inst Voor Plasma, NETHERLANDS
Prof. B.S. Liley, University of Waikato, NEW ZEALAND
Dr. Suresh C. Sharma, Univ of Calabar, NIGERIA
Prof. J.A.C. Cabral, Inst Superior Tech, PORTUGAL
Dr. Octavian Petrus, ALI CUZA University, ROMANIA
Prof. M.A. Hellberg, University of Natal, SO AFRICA
Dr. Johan de Villiers, Atomic Energy Bd, SO AFRICA
Fusion Div, Library, JEN, SPAIN
Prof. Hans Wilhelmson, Chalmers Univ Tech, SWEDEN
Dr. Lennart Stenflo, University of UMEA, SWEDEN
Library, Royal Inst Tech, SWEDEN
Dr. Erik T. Karlson, Uppsala Universitet, SWEDEN
Centre de Recherchesen, Ecole Polytech Fed, SWITZERLAND
Dr. W.L. Weise, Nat'l Bur Stand, USA
Dr. W.M. Stacey, Georg Inst Tech, USA
Dr. S.T. Wu, Univ Alabama, USA
Prof. Norman L. Oleson, Univ S Florida, USA
Dr. Benjamin Ma, Iowa State Univ, USA
Prof. Magne Kristiansen, Texas Tech Univ, USA
Dr. Raymond Askew, Auburn Univ, USA
Dr. V.T. Tolok, Kharkov Phys Tech Ins, USSR
Dr. D.D. Ryutov, Siberian Acad Sci, USSR
Dr. G.A. Eliseev, Kurchatov Institute, USSR
Dr. V.A. Glukhikh, Inst Electro-Physical, USSR
Institute Gen. Physics, USSR
Prof. T.J. Boyd, Univ College N Wales, WALES
Dr. K. Schindler, Ruhr Universitat, W. GERMANY
Nuclear Res Estab, Julich Ltd, W. GERMANY
Librarian, Max-Planck Institut, W. GERMANY
Dr. H.J. Kaeppler, University Stuttgart, W. GERMANY
Bibliothek, Inst Plasmaforschung, W. GERMANY